Comparison Study on SS and Double-Sided LCC Compensation Topologies for EV/PHEV Wireless Chargers

Weihan Li, *Student Member, IEEE*, Han Zhao, Junjun Deng, *Member, IEEE*, Siqi Li, *Member, IEEE*, and Chunting Chris Mi, *Fellow, IEEE*

***Abstract*—This paper compares the characteristics of the series–series and double-sided Inductor-Capacitor-Capacitor (LCC) compensation topologies for electric vehicle (EV) wireless chargers. Both the well-tuned and mistuned topologies for the two compensation methods are analyzed in detail. The mistuning considered here is mainly caused by the variations of the relative position between the primary and secondary sides. The output power displacements caused by mistuning are compared for both compensation topologies, as well as the impacts of the load variations on the performances of the mistuned topologies. The voltage and current stresses on components are also studied. The comparative result shows that the double-sided LCC compensation topology is less sensitive to mistuning. A double-sided LCC-compensated EV wireless charger system with up to 7.7-kW output power is built to verify the analysis results. A peak efficiency of 96% from dc power source to battery load is achieved.**

***Index Terms*—Compensation topology, electric vehicle (EV), inductive power transfer, mistuning, wireless charger.**

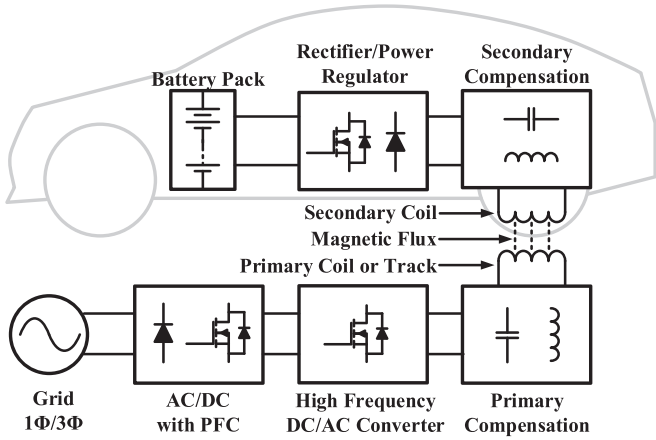

Fig. 1. Typical EV wireless charging system conceptual diagram.

I. Introduction

WIRELESS charging is gaining recognition as a preferred charging method for electric vehicles (EVs) [1]–[6] due to its advantages of convenience, safety, reliability, and weather-proof features. There are three types of wireless charging for EVs or plug-in hybrid EVs (PHEVs): static wireless charging, in which parked cars are charged; semidynamic charging, in which decelerating cars before traffic signals are charged or cars are charged opportunistically; and dynamic charging, in which normally running vehicles are charged [5], [7], [8]. A typical EV/PHEV wireless charging system is shown in Fig. 1. It consists of an ac/dc converter with power factor correction, a high-frequency dc/ac converter, primary and secondary coils with compensation circuits, and a rectifier or a power regulator with a filter [9]. Distinguishing from traditional conductive chargers (usually plug-in), the wireless charger takes advantage of the alternating magnetic field within a large gap to transfer power instead of physical connection or a regular transformer.

There are many research fields in wireless power transfer (WPT), such as compensation network and circuit analyses [10]–[12], coil design techniques for large gap and misalignment tolerance [8], [13], [14], optimization for high efficiency [15]–[17], control methods [18]–[20], foreign object detection, and safety issues. Among them, the compensation method is essential because of its functions of adjusting resonant frequency, minimizing the volt-ampere rating of power supply, improving coupling and power transfer capability, and achieving high efficiency [9], [12], [21]. It is well known that four basic compensation topologies, namely, series–series (SS), SP, PS, and PP, are widely adopted for EV applications. They are named by the way the compensated capacitors are connected to the primary and secondary coils. The first S or P represents the capacitor in series or parallel with the primary coil, and the second S or P stands for the capacitor in series or parallel with the

Manuscript received January 19, 2015; revised May 28, 2015 and August 30, 2015; accepted September 13, 2015. Date of publication September 25, 2015; date of current version June 16, 2016. This work was supported in part by a U.S. Department of Energy Graduate Automotive Technology Education Grant, by the U.S.–China Clean Energy Research Center—Clean Vehicle Consortium, by the University of Michigan, by Hefei University of Technology, and by the China Scholarship Council. The review of this paper was coordinated by Dr. K. Nam.

W. Li is with the School of Mechanical and Automotive Engineering, Hefei University of Technology, Hefei 230009, China, and also with the Department of Electrical and Computer Engineering, University of Michigan, Dearborn, MI 48128 USA (e-mail: weihanli1988@gmail.com).

H. Zhao is with the School of Mechanical and Automotive Engineering, Hefei University of Technology, Hefei 230009, China.

J. Deng is with the School of Automation, Northwestern Polytechnical University, Xi'an 710072, China (e-mail: dengjunjun1985@gmail.com).

S. Li is with the Department of Electrical Engineering, Kunming University of Science and Technology, Kunming 650500, China (e-mail: lisiqi00@gmail.com).

C. C. Mi is with the Department of Electrical and Computer Engineering, University of Michigan, Dearborn, MI 48128 USA (e-mail: chrismi@umich.edu).

Color versions of one or more of the figures in this paper are available online at http://ieeexplore.ieee.org.

Digital Object Identifier 10.1109/TVT.2015.2479938

secondary coil [12]. A comprehensive analysis of these basic topologies can be found in [6], [11], and [22]. Among these four topologies, only the SS compensation topology, which was analyzed in detail in [15], has the characteristics that the resonant frequency is independent of the coupling coefficient and load. This feature is essential for EV/PHEV application, particularly for semidynamic and dynamic charging. Because the coupling coefficient varies along with the change in the relative position between primary and secondary coils regardless of how good a driver's parking or driving skills are, the load also changes along with the battery charging time.

Many other novel compensation topologies were proposed as well; however, not all of them have the same characteristics as SS compensation topologies do. In [23], an inductor/capacitor/inductor (LCL) resonant circuit for the primary side was applied for WPT. However, the resonant frequency changes with variations of the coupling coefficient and load condition, and it did not present the method to design these three parameters. In [24] and [25], the LCL and capacitor/inductor/capacitor/inductor (CLCL) networks are applied in both primary and secondary sides, respectively. The resonant frequency is independent of the coupling coefficient and load condition. However, these two papers just focused on model and control, and the inductances of the additional inductors are equal to or larger than the inductances of the main coils in these topologies. A double-sided LCC compensation topology, whose additional inductors are smaller than the inductances of the main coils, was analyzed in [21]. It has similar characteristics with the double-sided LCL or CLCL topologies. In that paper, comprehensive characteristics had been presented, and the zero voltage switching (ZVS) condition had been realized. The last three compensation topologies have similar characteristics as SS compensation topologies; however, a clear comparison of SS compensation topologies with these topologies is not presented.

To reduce the reluctance, ferromagnetic material is usually used to concentrate the flux lines in practice [26]. As a result, the self-inductances of the primary and secondary coils slightly change when the relative position of the primary and secondary sides changes [26], [27]. Moreover, both inductors and capacitors always have tolerances during manufacturing. These will lead to the mistuning of the wireless charger resonant network.

In this paper, it mainly presents the comparison between the SS and the double-side LCC compensation topologies, in terms not only of the well-tuned system but of the mistuned system as well. The output power displacement factor (PDF) is defined as one criterion to quantify the impact of the mistuning. The voltage and current stresses on series capacitors and coils are studied. The impact of the mistuning when the load varies is also analyzed. All of the components are considered as ideal unless explicitly stated. The diodes of the rectifier at the secondary side are operated at continuous mode under most operating conditions, and only the fundamental harmonic is considered.

This paper is organized as follows. The analysis and basic characteristics of well-tuned and mistuned SS compensation topologies are presented in Section II. The model and basic characteristics of well-tuned and mistuned double-sided LCC compensation topologies are analyzed in Section III. The comparison between these two topologies is mainly conducted in Section IV. The experimental results of a prototype of the double-sided LCC-compensated wireless charger are presented in Section V. Finally, the conclusions are drawn in Section VI.

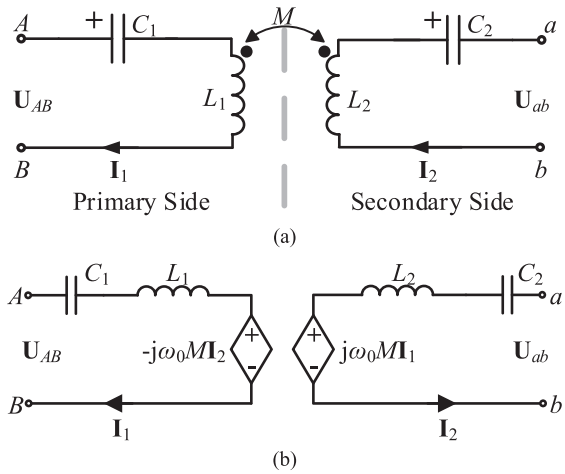

Fig. 2. SS compensation topology and modeling. (a) SS compensation topology. (b) Dependent voltage equivalent circuit model.

II. Characteristics of the Series–Series Compensation Topology

A. Basic Characteristics of the SS Compensation Topology

The SS compensation topology is shown in Fig. 2(a). For the dependent voltage equivalent circuit model in Fig. 2(b), the compensation capacitors (C_1 and C_2) are elaborately selected to resonate with the self-inductances (L_1 and L_2) in the primary and secondary sides, respectively. Thus

$$C_1 = \frac{1}{(\omega_0^2 L_1)} \tag{1}$$

$$C_2 = \frac{1}{(\omega_0^2 L_2)} \tag{2}$$

where ω_0 is the resonant frequency that is only related to the self-inductance and compensated capacitance.

In practice, the battery will be connected with nodes a and b through a rectifier and a filter. The battery to be charged is similar to a passive voltage source. Voltage $\mathbf{U}_{ab}$ between nodes a and b is the equivalent battery voltage and in phase with current $\mathbf{I}_2$, if the diodes of the rectifier are working at continuous mode, and only fundamental harmonic is considered in a circuit system consisting of entirely ideal components. By Kirchhoff's laws and with input voltage $\mathbf{U}_{AB}$ taken as the reference, the following equations can be readily observed:

$$\mathbf{I}_1 = \frac{\mathbf{U}_{ab}}{j\omega_0 M} = \frac{U_{ab}}{\omega_0 M}\angle 0^\circ \tag{3}$$

$$\mathbf{I}_2 = -\frac{\mathbf{U}_{AB}}{j\omega_0 M} = \frac{U_{AB}}{\omega_0 M}\angle 90^\circ. \tag{4}$$

It is generally known, and can be also found in (4), that the root mean square (RMS) value of the output current $\mathbf{I}_2$ is independent of the output voltage if the input voltage, mutual inductance, and other circuit parameters stay the same. The SS-compensated wireless charger is a constant current source

and can be controlled by the input voltage in practice. The output current $\mathbf{I}_2$, which is in phase with output voltage $\mathbf{U}_{ab}$, is 90° ahead of input voltage $\mathbf{U}_{AB}$. Similar characteristics can be found for input current $\mathbf{I}_1$, which is independent of the RMS value of input voltage $\mathbf{U}_{AB}$ but is in phase with it.

Based on the previous assumptions and analysis, for the SS-compensated wireless charger system with ideal components, there is no reactive power in the system, and the power factor PF is unity. The output and input real power can be obtained as

$$P_{\text{out\_tuned}} = P_{\text{in\_tuned}} = \text{Re}\left(\mathbf{U}_{AB}\mathbf{I}_1^*\right) = \frac{1}{\omega_0 M} U_{AB} U_{ab} \quad (5)$$

where $\mathbf{I}_1^*$ refers to the complex conjugate of $\mathbf{I}_1$.

It is important to note that the input current, output current, and power are inversely proportional to the mutual inductance. Generally, the mutual inductance will reduce when the primary and secondary coils are misaligned. The more they are misaligned, the smaller the mutual inductance is. For EV/PHEV applications, it can be known literally from (3)–(5) that the input current, output current, and power will be very large if the car is charged when it is stopped away from the central position. Moreover, to keep the same output power, the input current should be larger with a smaller mutual inductance, which will lead to a reduction in efficiency. Therefore, position detection is very important for the SS-compensated wireless charger to ensure the mutual inductance M within a certain scope.

B. Basic Characteristics of the Mistuned SS Compensation Topology

The variation in the primary or secondary inductance ΔL_i is defined by

$$\Delta L_i = L_i - L_{i0} \quad (6)$$

where $i = 1$ stands for the primary side, $i = 2$ stands for the secondary side, L_i is the actual inductance at current position, and L_{i0} is the nominal inductance when the primary and secondary sides are perfectly aligned.

For the SS-compensated resonant tank, the variation of capacitance ΔC_i can be equivalent to the variation of inductance on the same side $\Delta L_i'$, assuming that the operating frequency is the nominal resonant frequency ω_0. Thus

$$\Delta L_i' = \frac{\Delta C_i}{\omega_0^2 C_i (C_i + \Delta C_i)}. \quad (7)$$

Hence, it is reasonable to only consider the variations of the inductances in this analysis.

The equivalent circuit of a wireless charger resonant tank with mistuned series-compensated primary and secondary sides is shown in Fig. 3.

Based on Kirchhoff's laws, the following equations can be obtained:

$$\mathbf{I}_1 = \frac{1}{j\omega_0 \left(M - \Delta L_1 \Delta L_2 / M\right)} \left(\mathbf{U}_{ab} - \frac{\Delta L_2}{M} \cdot \mathbf{U}_{AB}\right) \quad (8)$$

$$\mathbf{I}_2 = \frac{1}{j\omega_0 \left(M - \Delta L_1 \Delta L_2 / M\right)} \left(\mathbf{U}_{ab} \cdot \frac{\Delta L_1}{M} - \mathbf{U}_{AB}\right). \quad (9)$$

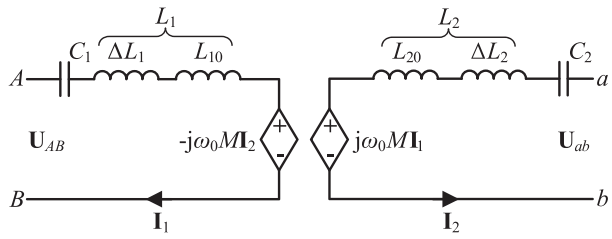

Fig. 3. Mistuned SS compensation topology equivalent circuit model.

By comparing (8) and (9) with (3) and (4), respectively, we can find that if the considered variations of the self-inductances are caused by the misalignment, the mutual inductance will always be involved and coupled with them. To clearly express the mistune effect, the term $\delta_i (\delta_i = \Delta L_i / M)$ is introduced here. It is the ratio of the variation of self-inductance over mutual inductance. As the assumptions have been set in Section II-A, output voltage $\mathbf{U}_{ab}$ is in phase with output current $\mathbf{I}_2$, and input voltage $\mathbf{U}_{AB}$ is taken as the reference. Referring to $\mathbf{U}_{AB}$, φ is defined as the phase of output voltage $\mathbf{U}_{ab}$, and α is the phase of input current $\mathbf{I}_1$. Then, (8) and (9) can be rewritten as

$$\mathbf{I}_1 = \frac{1}{1 - \delta_1 \delta_2} \left| \frac{\sin\varphi}{\cos\alpha} \right| \frac{U_{ab}}{\omega_0 M} \angle\alpha \quad (10)$$

$$\mathbf{I}_2 = \frac{|\sin\varphi|}{1 - \delta_1 \delta_2} \frac{U_{AB}}{\omega_0 M} \angle\varphi. \quad (11)$$

The output and input real power of the mistuned system can be expressed as

$$\begin{aligned} P_{\text{out\_mistuned}} = P_{\text{in\_mistuned}} &= \text{Re}\left(\mathbf{U}_{AB}\mathbf{I}_1^*\right) \\ &= \frac{1}{\omega_0 M} U_{AB} U_{ab} \frac{|\sin\varphi|}{1 - \delta_1 \delta_2} \end{aligned} \quad (12)$$

where φ and α are determined by

$$\cos\varphi = \frac{\Delta L_1}{M} \cdot \frac{U_{ab}}{U_{AB}} = \delta_1 \cdot G_V \quad (13)$$

$$\tan\alpha = \frac{-G_V^2 \delta_1 + \delta_2}{G_V \sqrt{1 - G_V^2 \delta_1^2}} \quad (14)$$

where $G_V = U_{ab}/U_{AB}$ is the voltage gain, and the power factor PF is given as

$$PF = \cos\alpha = \sqrt{\frac{G_V^2 \left(1 - G_V^2 \delta_1^2\right)}{G_V^2 + \delta_2^2 - 2 G_V^2 \delta_1 \delta_2}}. \quad (15)$$

It is obvious that phase φ only depends on δ_1 and G_V; α, and the power factor only relates to δ_1, δ_2 and G_V. The RMS values of the current and power relate to δ_1, δ_2 and G_V, as well apart from the main factor M.

Compared with the perfectly tuned resonant tank analyzed in Section II-A, it is different in both the amplitudes and phases of input current and output current (phase difference for output voltage) for the mistuned system, as the ratio of the variation of the inductances over mutual inductance (δ_i) is a critical factor,

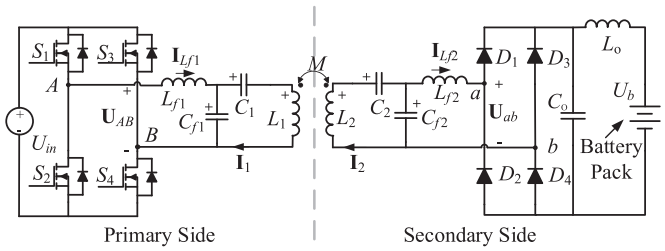

Fig. 4. Double-sided LCC compensation topology.

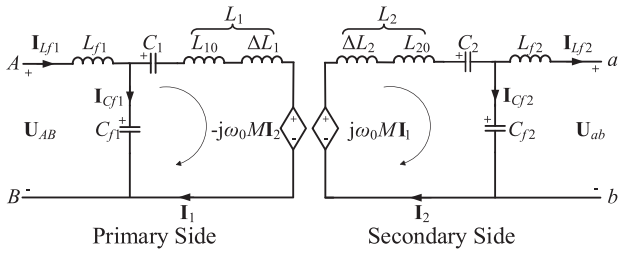

Fig. 5. Mistuned double-sided LCC compensation topology equivalent circuit model.

and it is not the only cause of the difference. The difference is also determined by the voltage gain (G_V), which determines the phase angle φ and α together with δ_i.

Generally, the variation of the self-inductance ΔL_i caused by the misalignment is negative if the nominal self-inductance L_{i0} is defined on the condition of the primary and secondary sides with perfect alignment. Hence, it is easy to determine that $90^\circ < \varphi < 180^\circ$ in (13). For an SS system with symmetrical primary and secondary sides, ΔL_1 and ΔL_2 are quite small and very close. It is reasonable to assume that $\Delta L_1 = \Delta L_2$. Hence, the following conclusions can be obtained from (14) and (15) if the symmetrical SS system is operated at the nominal resonant frequency ω_0 when there is a misalignment.

1) If $G_V = 1$ ($U_{ab} = U_{AB}$), then $\alpha = 0^\circ$ (the input current $\mathbf{I}_1$ and input voltage $\mathbf{U}_{AB}$ are in phase), the power factor $PF = 1$.
2) If $G_V > 1$ ($U_{ab} > U_{AB}$), then $0^\circ < \alpha < 90^\circ$ (the input current $\mathbf{I}_1$ is α degrees ahead of the input voltage $\mathbf{U}_{AB}$), the power factor $PF = \cos\alpha$.
3) If $G_V < 1$ ($U_{ab} < U_{AB}$), then $-90^\circ < \alpha < 0^\circ$ (the input current $\mathbf{I}_1$ lags the input voltage $\mathbf{U}_{AB}$ by α degrees), the power factor $PF = \cos\alpha$.

For the third point, it makes a contribution to ZVS realization. To realize ZVS turn-on for a metal–oxide–semiconductor field-effect transistor (MOSFET), the MOSFET body diode should conduct before the MOSFET does. This requires the parasitic capacitor to be discharged before the current becomes positive [28]. For a full-bridge inverter, it requires that the current lags the voltage to realize ZVS switching for all MOSFETs [21]. Hence, for an SS system with symmetrical primary and secondary sides, the condition, i.e., $G_V < 1$ ($U_{ab} < U_{AB}$), contributes to MOSFETs ZVS realizing when the misalignment happens, although it leads to additional reactive power in the system.

III. Characteristics of the Double-Sided LCC Compensation Topology

A. Basic Characteristics of the Double-Sided LCC Compensation Topology

The double-sided LCC compensation topology (as shown in Fig. 4) has been extensively researched in recent years. This topology has an additional series inductor and an additional parallel capacitor for both primary and secondary sides compared with the SS compensation topology. Here, a symmetrical topology is considered. The basic characteristics can be referred to [21]. The following equations can be readily obtained:

$$\omega_0 = \frac{1}{\sqrt{L_{f1}\cdot C_{f1}}} = \frac{1}{\sqrt{L_{f2}\cdot C_{f2}}} = \frac{1}{\sqrt{(L_1 - L_{f1})\cdot C_1}} = \frac{1}{\sqrt{(L_2 - L_{f2})\cdot C_2}} \tag{16}$$

$$\mathbf{I}_{Lf1} = \frac{M\mathbf{U}_{ab}}{j\omega_0 L_{f1}L_{f2}} = \frac{MU_{ab}}{\omega_0 L_{f1}L_{f2}}\angle 0^\circ \tag{17}$$

$$\mathbf{I}_1 = \frac{\mathbf{U}_{AB}}{j\omega_0 L_{f1}} = \frac{U_{AB}}{\omega_0 L_{f1}}\angle -90^\circ \tag{18}$$

$$\mathbf{I}_2 = -\frac{\mathbf{U}_{ab}}{j\omega_0 L_{f2}} = \frac{U_{ab}}{\omega_0 L_{f2}}\angle 0^\circ \tag{19}$$

$$\mathbf{I}_{Lf2} = \frac{M\mathbf{U}_{AB}}{j\omega_0 L_{f1}L_{f2}} = \frac{MU_{AB}}{\omega_0 L_{f1}L_{f2}}\angle -90^\circ \tag{20}$$

$$P_{\text{out\_tuned}} = P_{\text{in\_tuned}} = \text{Re}\left(\mathbf{U}_{AB}\mathbf{I}^*_{Lf1}\right) = \frac{M}{\omega_0 L_{f1}L_{f2}}U_{AB}U_{ab} \tag{21}$$

where $\mathbf{I}^*_{Lf1}$ refers to the complex conjugate of $\mathbf{I}_{Lf1}$.

It is obvious that the resonant frequency is only related to inductances and capacitances, independent of coupling and the load condition. The input current $\mathbf{I}_{Lf1}$ is in phase with input voltage $\mathbf{U}_{AB}$, and its amplitude is related to output voltage U_{ab}; the output current I_{Lf2} is determined by input voltage U_{AB} if the relative position of the primary and secondary sides is known. The current on the primary coil I_1 is also determined by input voltage U_{AB}, which is irrelevant to the load and is essential for multisecondary applications. Differently from the SS compensation topology, the transferred power, input current, and output current are proportional to mutual inductance M.

Generally, the maximum power transfer capability of the uncompensated secondary coil is limited. Different compensation methods can achieve different maximum transferred power levels. Apart from the input and output voltages, mutual inductance M and resonant frequency ω_0 are the two determining factors. However, the mutual inductance usually is limited due to the limited coil sizes, gap distance, possible misalignment, and efficiency requirement. The resonant frequency is also restricted by current power electronics technology and some standards (e.g., SAE-J2954). For the double-sided LCC compensation topology, L_{f1} or L_{f2} can be used as another design consideration to design a wireless charger system with proper power and efficiency.

B. Basic Characteristics of the Mistuned Double-Sided LCC Compensation Topology

The equivalent circuit of the mistuned double-sided LCC compensation topology is shown in Fig. 5. Based on the same

assumptions of the mistuned SS compensation and Kirchhoff's laws, the following equations can be obtained:

$$\begin{aligned}\mathbf{I}_{Lf1} &= -\frac{M}{j\omega_0 L_{f1}L_{f2}}\mathbf{U}_{ab} - \frac{\Delta L_1}{j\omega_0 L_{f1}^2}\mathbf{U}_{AB} \\ &= \frac{MU_{ab}}{\omega_0 L_{f1}L_{f2}}\left|\frac{\sin\varphi}{\cos\alpha}\right|\angle\alpha \qquad (22)\\ \mathbf{I}_1 &= \frac{\mathbf{U}_{AB}}{j\omega_0 L_{f1}} = \frac{U_{AB}}{\omega_0 L_{f1}}\angle -90^\circ \qquad (23)\\ \mathbf{I}_2 &= -\frac{\mathbf{U}_{ab}}{j\omega_0 L_{f2}} = \frac{U_{ab}}{\omega_0 L_{f2}}\angle 90^\circ + \varphi \qquad (24)\\ \mathbf{I}_{Lf2} &= \frac{M}{j\omega_0 L_{f1}L_{f2}}\mathbf{U}_{AB} + \frac{\Delta L_2}{j\omega_0 L_{f2}^2}\mathbf{U}_{ab} \\ &= \frac{MU_{AB}}{\omega_0 L_{f1}L_{f2}}|\sin\varphi|\angle\varphi \qquad (25)\\ P_{\text{out\_mistuned}} &= P_{\text{in\_mistuned}} = \text{Re}\left(\mathbf{U}_{AB}\mathbf{I}_{Lf1}^*\right) \\ &= \frac{M}{\omega_0 L_{f1}L_{f2}}U_{AB}U_{ab}|\sin\varphi| \qquad (26)\end{aligned}$$

where φ is the phase of output voltage $\mathbf{U}_{ab}$, and α is the phase of input current $\mathbf{I}_{Lf1}$. They can be obtained by the following equations:

$$\cos\varphi = -\frac{L_{f1}}{L_{f2}}\frac{\Delta L_2}{M}\frac{U_{ab}}{U_{AB}} = -m_f\cdot\delta_2\cdot G_V \qquad (27)$$

$$\tan\alpha = \frac{\delta_1 - m_f^2\delta_2 G_V^2}{m_f G_V\sqrt{1-m_f^2\delta_2^2 G_V^2}}. \qquad (28)$$

It is easy to determine that $-180^\circ < \varphi < -90^\circ$ if the variation of the self-inductance is negative.

IV. Comparison Between the Double-Sided LCC and Series–Series Compensation Topologies

The given analysis has already shown some similarities and differences between the double-sided LCC and SS compensation topologies in the basic characteristics of not only the two well-tuned topologies but the two mistuned topologies as well.

For similarities, there are two main points. One is that the resonant frequencies are independent of the coupling and load condition for both compensation topologies. The other point is that both topologies are current sources; the output currents are irrelevant to the load condition (output voltage) and only dependent on the input voltage, resonant frequency, and mutual inductance.

However, the differences are more significant. First, the SS compensation topology needs fewer components than the double-sided LCC compensation topology. This is one of the advantages of the SS compensation topology. Second, the output power of the SS compensation topology increases with the decrease in the mutual inductance. This requires the SS-compensated wireless charger to be equipped with position detection technology or maximum output power limit protection for safety concerns. However, this is not necessary for the double-sided LCC-compensated wireless charger because of the characteristics that the transferred power decreases with the decreasing of the mutual inductance. The maximum transferred power will be achieved when the primary and secondary sides are well aligned. Third, the output power of the SS-compensated wireless charger will be determined when the resonant frequency, coil structure, and misalignment tolerance are given. However, in the double-sided LCC-compensated wireless charger system, the additional inductances L_{f1} and L_{f2} can work as extra parameters to adjust the output power. Fourth, the current on the primary coil of the double-sided LCC-compensated wireless charger is also constant and only determined by the input voltage. This is important for a multi-receiver wireless charger system. Some of the characteristics of both topologies are listed in Table I.

However, it cannot be easily identified which topology is better. To compare these two topologies, more aspects should be considered, such as the output power displacement (PD), voltage and current stresses on components, and efficiency.

A. Output PDF

The output PDF is defined as

$$\text{PDF} = \frac{P_{\text{out\_mistuned}} - P_{\text{out\_tuned}}}{P_{\text{out\_tuned}}} \qquad (29)$$

where $P_{\text{out\_tuned}}$ is the output power of the well-tuned wireless charging system, and $P_{\text{out\_mistuned}}$ is the output power of the mistuned wireless charging system. The output PDF shows how much output power the mistuned topology deviates from the well-tuned topology. As previously mentioned, the characteristics of the mistuned system are affected by the variations of the self-inductances coupled with the change in mutual inductance if there is a misalignment. Hence, here, we also use the term δ_i to represent the inductance change factor (self-inductance and mutual inductance) caused by the misalignment. The output PDF will be expressed by δ_i. For the SS compensation topology, we obtain

$$\begin{aligned}\text{PDF}_{SS} &= \frac{\sqrt{1-G_V^2\cdot\left(\frac{\Delta L_1}{M}\right)^2}}{1-\frac{\Delta L_1\Delta L_2}{M^2}} - 1 = \frac{\sqrt{1-G_V^2\cdot\delta_1^2}}{1-\delta_1\delta_2} - 1 \\ &= \left|\frac{\sin\varphi}{1-\delta_1\delta_2}\right| - 1. \qquad (30)\end{aligned}$$

For the double-sided LCC compensation topology, we obtain

$$\begin{aligned}\text{PDF}_{LCC} &= \sqrt{1-m_f^2G_V^2\left(\frac{\Delta L_2}{M}\right)^2} - 1 = \sqrt{1-m_f^2G_V^2\delta_2^2} - 1 \\ &= |\sin\varphi| - 1. \qquad (31)\end{aligned}$$

Here, the critical output PDF $CPDF$ is defined when $m_f = 1$, $\delta_1 = \delta_2$, and $G_V = 1$. It is obvious that

$$CPDF_{SS} = \frac{1}{|\sin\varphi|} - 1 \text{ or } \frac{1}{\sqrt{1-\delta_i^2}} - 1 \qquad (32)$$

$$CPDF_{LCC} = |\sin\varphi| - 1 \text{ or } \sqrt{1-\delta_i^2} - 1. \qquad (33)$$

Obviously, $CPDF_{SS}$ is positive, and $CPDF_{LCC}$ is negative. The absolute value of the critical output power of the SS compensation topology $CPDF_{SS}$ is larger than that of

TABLE I
COMPARISON BETWEEN THE SS AND DOUBLE-SIDED LCC COMPENSATION TOPOLOGIES

	Items		SS Compensation Topology	LCC Compensation Topology
	P_{out_tuned}		$\frac{1}{\omega_0 M} U_{AB} U_{ab}$	$\frac{M}{\omega_0 L_{f1} L_{f2}} U_{AB} U_{ab}$
$\Delta L_i<0$	$P_{out\_mistuned}$		$\frac{\lvert\sin\varphi\rvert}{1-\delta_1\delta_2}\cdot\frac{1}{\omega_0 M}\cdot U_{AB}U_{ab}$	$\lvert\sin\varphi\rvert\cdot\frac{M}{\omega_0 L_{f1}L_{f2}}\cdot U_{AB}U_{ab}$
	φ	$\Delta L_i\neq 0$	$90°<\varphi<<180°$	$-180°<<\varphi<-90°$
		$\Delta L_1\neq 0$, $\Delta L_2=0$	$90°<\varphi<<180°$	$-90°$
		$\Delta L_1=0$, $\Delta L_2\neq 0$	$90°$	$-180°<<\varphi<-90°$
	$\cos\varphi$		$\delta_1\cdot G_V$	$-m_f\cdot G_V\cdot\delta_2$
	α ($\Delta L_1=\Delta L_2$)	$U_{ab}=U_{AB}$	$0°$	$0°$
		$U_{ab}>U_{AB}$	$0°<\alpha<<90°$	$-90°<<\alpha<0°$
		$U_{ab}<U_{AB}$	$-90°<<\alpha<0°$	$0°<\alpha<<90°$
	$\tan\alpha$		$\frac{-G_V^2\delta_1+\delta_2}{G_V\sqrt{1-G_V^2\delta_1^2}}$	$\frac{\delta_1-m_f^2G_V^2\delta_2}{m_fG_V\sqrt{1-m_f^2G_V^2\delta_2^2}}$
	PF ($\cos\alpha$)		$\sqrt{\frac{G_V^2(1-G_V^2\delta_1^2)}{G_V^2+\delta_2^2-2G_V^2\delta_1\delta_2}}$	$\sqrt{\frac{m_f^2G_V^2(1-m_f^2G_V^2\delta_2^2)}{m_f^2G_V^2+\delta_1^2-2m_f^2G_V^2\delta_1\delta_2}}$
	PDF		$\left\lvert\frac{\sin\varphi}{1-\delta_1\delta_2}\right\rvert-1$	$\lvert\sin\varphi\rvert-1$
	$CPDF$ (m_f=1, $\Delta L_1=\Delta L_2$,G_V=1)		$\left\lvert\frac{1}{\sin\varphi}\right\rvert-1$ or $\frac{1}{\sqrt{1-\delta_i^2}}-1$	$\lvert\sin\varphi\rvert-1$ or $\sqrt{1-\delta_i^2}-1$

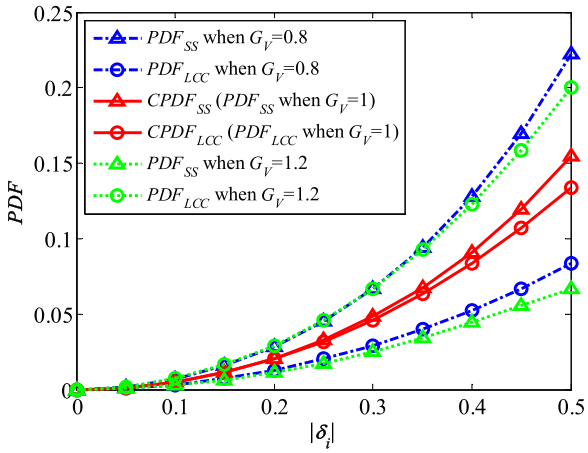

Fig. 6. Output PDF for the SS and double-sided LCC compensation topology at different loads (different voltage gains G_V).

the LCC compensation topology $CPDF_{LCC}$. The former is $1/|\sin\varphi|$ times of the latter. As shown in Fig. 6, the output PDF of the double-sided LCC compensation topology is less than that of the SS compensation topology when $G_V <= 1$. The situation reverses when $G_V > 1$. The battery-charging process usually consists of a constant-current charging stage and a constant-voltage charging stage. The battery voltage will increase with time during the constant-current stage. During this stage, the input voltage is usually larger than the battery voltage. After the battery voltage reaches its maximum, it will go to the constant-voltage stage, and the charging current will drop with time. Hence, $G_V <= 1$ is preferred if the constant-current stage is the main stage of the battery-charging process. The double-sided LCC compensation topology is better than the SS compensation topology from this point of view.

B. Stresses on the Components

It is difficult to compare the stresses on the components and efficiency if the variations of mutual inductance and self-inductances are considered at the same time. Here, only the mutual inductance is taken into consideration since it is the main factor that impacts the output power. It is easy to know that the voltage and current stresses over L_1 and L_2 are the same if the SS and double-sided LCC-compensated wireless charging systems are designed to transfer the same amount of power only at the aligned position. On the other hand, the voltage stresses over C_1 and C_2 of the double-sided LCC-compensated system are smaller, only $(L_i - L_{fi})/L_i$ times of those of the SS-compensated system if $G_V = 1$. Obviously, the efficiency of the SS-compensated system is higher than that of the double-sided LCC-compensated system since additional components L_{f1}, L_{f2}, C_{f1}, and C_{f2} are used.

A better idea is to compare them based on the premise that the two systems are designed to transfer certain power within a certain misalignment scope. Hence, the SS-compensated WPT is designed to transfer nominal power at the perfectly aligned position, whereas the double-sided LCC-compensated WPT is designed at the maximum misaligned position. Assuming that $L_{f1} = L_{f2}$ for a symmetrical system, M_m is the maximum mutual inductance when the coils are aligned, and M_n is the minimum mutual inductance when the system is at its maximum misaligned position. Hence, from (5) and (21), the following equation can be obtained:

$$L_{f1} = L_{f2} = \sqrt{M_m M_n}. \tag{34}$$

By changing the input voltage, the transferred power is controlled to stay at the rated value while misalignment exists. The

relationship between input voltage U_{AB} and mutual inductance M is illustrated by the following equations:

$$U_{AB}^{SS} = \frac{M}{M_m} U_{ABm} \tag{35}$$

$$U_{AB}^{LCC} = \frac{M_n}{M} U_{ABm} \tag{36}$$

where U_{AB}^{SS} is the input RMS voltage of the SS-compensated system, U_{AB}^{LCC} is the input RMS voltage of the double-sided LCC-compensated system, and U_{ABm} is the maximum input RMS voltage.

It is obvious that, while transferring the rated power, the voltages and currents on the components of the secondary side are the same when the mutual inductance changes. The difference is just on the primary side. The RMS value of the current on C_1 and L_1 of the SS and double-sided LCC-compensated systems can be obtained from (3), (18), and (36). Thus

$$I_1^{SS} = \frac{U_{ab}}{\omega M} = \frac{P_O}{U_{ABm}} \frac{M_m}{M} \tag{37}$$

$$I_1^{LCC} = \frac{U_{AB}^{LCC}}{\omega L_{f1}} = \frac{U_{ABm}}{\omega L_{f1}} \frac{M_n}{M} \tag{38}$$

where I_1^{SS} is the RMS current on the coil L_1 of the SS-compensated system, I_1^{LCC} is the RMS current on the coil L_1 of the double-sided LCC-compensated system, and P_O is the rated power.

It is easy to get the RMS voltage on capacitor C_1 for both the SS and double-sided LCC compensation topologies, as follows:

$$U_{C_1}^{SS} = \frac{L_1}{M} U_{ab} = \omega L_1 \frac{P_O}{U_{ABm}} \frac{M_m}{M} \tag{39}$$

$$U_{C_1}^{LCC} = U_{ABm} \frac{L_1 - L_{f1}}{L_{f1}} \frac{M_n}{M} \tag{40}$$

$$\frac{U_{C_1}^{SS}}{U_{C_1}^{LCC}} = \frac{L_1 \sqrt{M_m M_n}}{\left(L_1 - \sqrt{M_m M_n}\right) M_n} \frac{U_{ab}}{U_{ABm}} \tag{41}$$

where U_{C1}^{SS} and U_{C1}^{LCC} are the RMS voltages on the capacitor C_1 of the SS and double-sided LCC compensation topologies, respectively. It is obvious that voltage stresses on C_1 of the SS and double-sided LCC compensation topologies relate to the coil structure, maximum misalignment, and the ratio of U_{ab} and U_{ABm}. In fact, the voltage stress on C_1 of the SS compensation topology is higher than that of the double-sided LCC compensation topology at the rated power since the maximum input voltage U_{ABm} is close to the output voltage U_{ab}.

C. Efficiency Comparison

Four more components, namely, L_{f1}, L_{f2}, C_{f1}, and C_{f2}, are used in the double-sided LCC compensation topology compared with the SS compensation topology. Due to the equivalent series resistance of the capacitors, copper loss and core loss of the inductors, and dissipative loss [29], these resonant inductors and capacitors in the main power paths will lower the efficiency if the input voltage and load are the same as the SS compensation topology. However, the situation will be different if the wireless charging systems are operated at the rated power with different misalignment levels. As previously mentioned, the SS-compensated WPT is designed to transfer nominal power when the mutual inductance is at maximum, whereas the double-sided LCC-compensated WPT is designed when the mutual inductance is at minimum. The output power is regulated by controlling the input voltage. When the mutual inductance is at maximum, the input voltage of the SS compensation topology will be higher than that of the double-sided LCC compensation topology according to (35) and (36). Then, the current of the SS compensation topology will be lower if transferring the nominal power. Hence, the efficiency of the SS compensation topology is higher when the mutual inductance is at maximum. On the other hand, the efficiency of the double-sided LCC compensation topology is higher when the mutual inductance is at minimum.

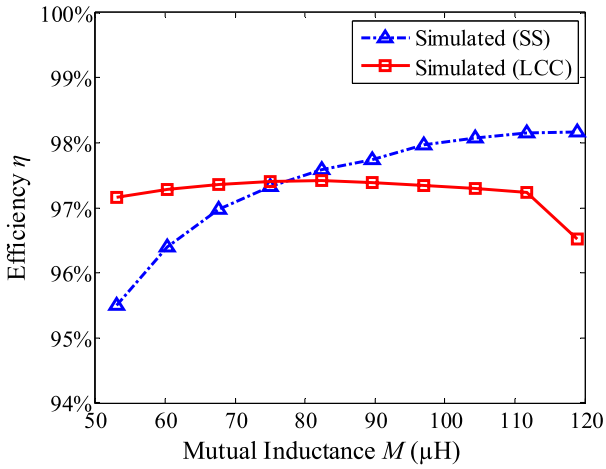

Fig. 7. Comparison of the simulated efficiency between the SS and double-sided compensation topologies at rated power from dc to dc.

Fig. 7 gives the simulated efficiency comparison between these topologies at the rated power from dc source to dc battery load. The efficiency of the double-sided LCC compensation topology is higher and steady, although it is lower than that of the SS compensation topology at higher mutual inductance values. The reason that the double-sided LCC compensation topology has a steady efficiency is that the loss on the compensation network increases while the loss on the primary coil decreases when the mutual inductance increases.

V. Experimental Results

The coil structure designed in [13] is adopted. The coil is 600 mm × 800 mm and was built using Litz wire (AWG38 – 800 strands). The ferrite bars are built from small ferrite pieces (TDK PC40). Other details of the coil can be found in the experimental setup (see Fig. 11). Fig. 8 shows the measured coil parameters. δ_i varies from -0.16 to 0. However, when considering the machining error, this value will be out of this range.

Assuming that the input square-wave voltage is 425 V, the battery voltage is from 300 to 450 V. The WPT system is always operated at the resonant frequency. According to (5), the minimum output power of the SS-compensated wireless

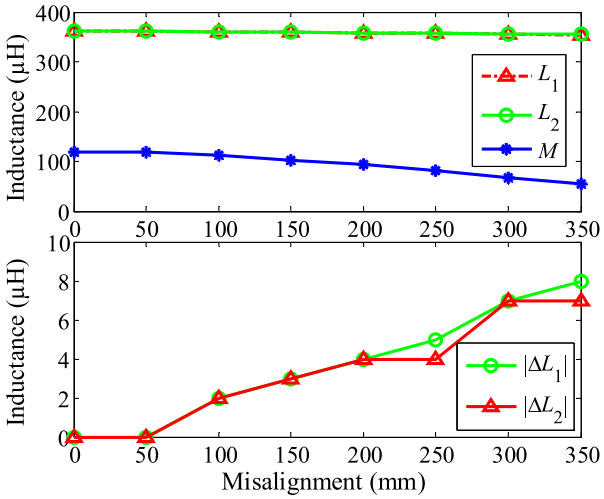

Fig. 8. Measured self-inductances, mutual inductance, and self-inductance variations at different misalignments.

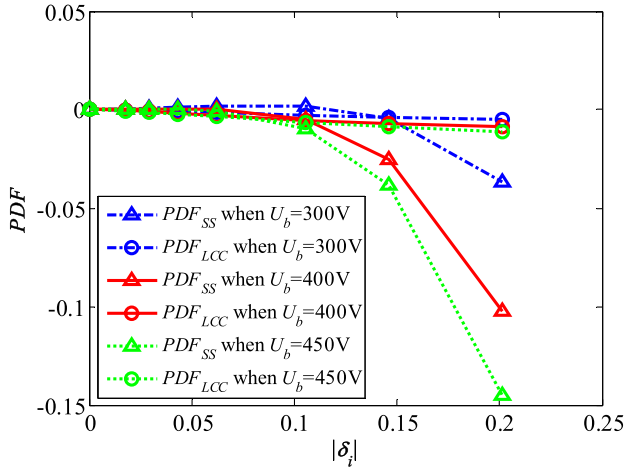

Fig. 9. Calculated output PDFs of the SS and double-sided LCC compensation topologies at different loads (different battery voltages) when the output power is 2.6 kW.

TABLE II
SPECIFICATION AND PARAMETERS OF THE SS AND DOUBLE-SIDED LCC-COMPENSATED WIRELESS CHARGER SYSTEM

Symbol	Spec/Parameter	LCC	SS
U_{AB}	RMS value of input voltage	<=383V	
U_{ab}	RMS value of output voltage	270V~405V	
f	Resonant frequency	79kHz	
P	Designed power	~2.6kW	
M	Mutual inductance	53μH~119μH	
L_{i0}[a]	Nominal self-inductances	360μH	
r_{Li}[a]	The AC resistance of the Main coil	~500mΩ	
C_1	Primary series capacitor	14.46nF	11.27nF
C_2	Secondary series capacitor	15.5nF[b]	10.6nF[b]
L_{fi}[a]	Additional inductors	79.4μH	/
r_{Lfi}[a]	The AC resistance of the Additional inductors	50 mΩ	/
C_{fi}[a]	Parallel capacitors	51.12nF	/

[a] i = 1, 2 stands for the primary and secondary respectively.
[b] C_2 is adjusted to achieve ZVS.

charger can be determined; it is only 2.6 kW, which is the rated power. To compare these two topologies at the same power level, the additional inductances L_{f1} and L_{f2} are designed to be 79.4 μH. The designed parameters are listed in Table II.

Fig. 9 shows that the calculated output PDFs of the double-sided LCC and SS compensation topologies change with $|\delta_i|$ for different battery voltages at the same output power, i.e., 2.6 kW. It is obvious that PDF_{LCC} slightly changes when both $|\delta_i|$ and battery voltage U_{ab} change. PDF_{LCC} is always negative, and the absolute value of PDF_{LCC} is less than 0.01. However, PDF_{SS} has a relative significant variation (even from positive to negative) when $|\delta_i|$ or battery voltage U_{ab} increases after $|\delta_i| > 0.05$. Hence, in this respect, the double-sided LCC compensation topology is also better than the SS compensation topology.

Simulation models of these two systems are built in LTspice mainly using the parameters in Table II. The calculated and

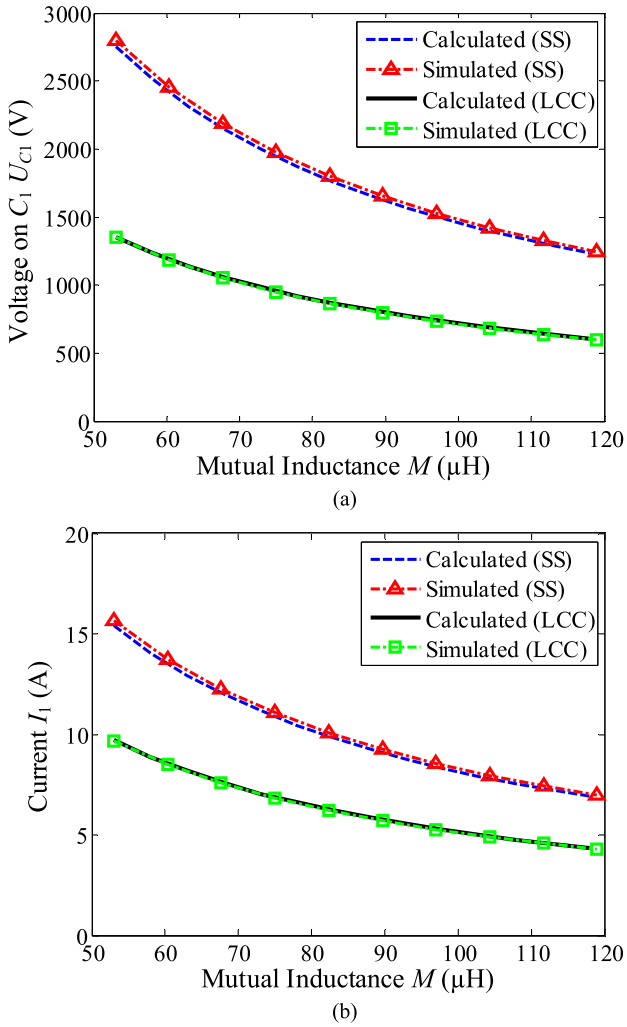

Fig. 10. Comparison of voltage and current stresses on components for the SS and double-sided LCC compensation topologies. (a) Voltage on primary series capacitor C_1. (b) Current on primary main coil L_1.

simulated voltage on C_1 and current of L_1 for both topologies are shown in Fig. 10. The calculated results are using the equations in Section IV and labeled as "Calculated ($*$)," whereas

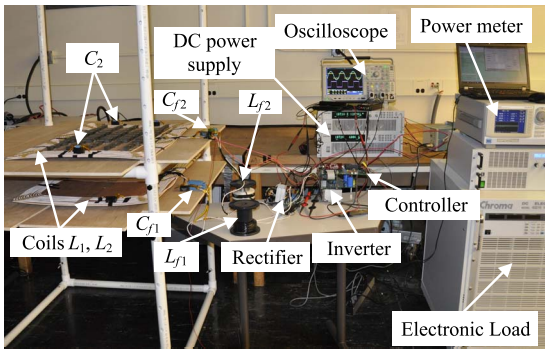

(a)

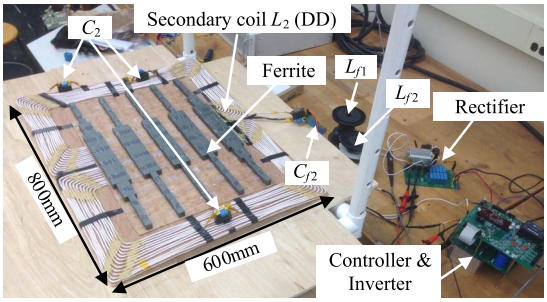

(b)

Fig. 11. Experimental setup for the double-sided LCC-compensated wireless charger system (from dc source to dc load). (a) Entire system setup. (b) Details of the coil and controller.

TABLE III
SPECIFICATION AND PARAMETERS OF THE DOUBLE-SIDED LCC-COMPENSATED WIRELESS CHARGER SYSTEM

Symbol	Spec/Parameter	Value [a]
U_{in}	Input DC voltage	<=425 V
U_b	Output battery voltage	300 V~450 V
f	Resonant frequency	79 kHz
	Nominal gap	200 mm
	Coil dimension	600x800mm
M	Mutual inductance	53 μH ~119 μH
L_{i0}[a]	Nominal self-inductances	360 μH
r_{Li}[a]	The AC resistance of the main coil	~500mΩ
ΔL_i[a]	Variations of self-inductances	0~8 μH [b]
C_1	Primary series capacitor	14 nF
C_2	Secondary series capacitor	15.1 nF
L_{fi}[a]	Additional inductors	67 μH
r_{Lfi}[a]	The AC resistance of the additional inductors	~50 mΩ
C_{fi}[a]	Parallel capacitors	60.6 nF
P	Designed power	~8kW

[a] i= 1, 2 stands for the primary and secondary respectively.

the simulated results are labeled as "Simulated (∗)." It can be seen that the LCC compensation topology is better than the SS compensation topology.

According to the given comparison and analysis, we can see that the power transfer capability of the double-sided LCC compensation topology is better than that of the SS compensation topology. The voltage and current stresses of the double-sided LCC compensation topology are lower than those of the SS

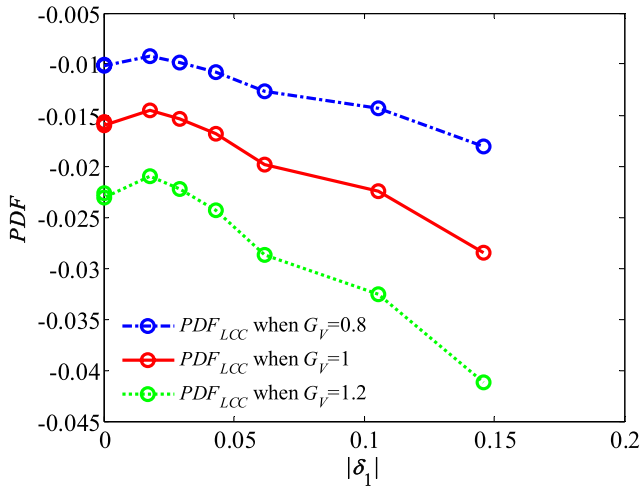

Fig. 12. Output power factor of the double-sided LCC-compensated wireless charger at different variations of the self-inductances and loads when an additional positive capacitance ΔC_2 is considered.

topology when charging the same battery at the rated power. Due to time and funding constraints, we only built the double-sided LCC compensation topology for a high-power wireless charging system. The wireless charger system experimental setup is shown in Fig. 11. The parameters are listed in Table III. The design method can be found in [21]. The variation of the secondary series capacitance ΔC_2 (positive) can be equivalent to the variation of the secondary main coil self-inductance $\Delta L_2'$ ($\Delta L_2' = 21\ \mu$H) as addressed by (7). It is obvious that $\delta_1 = 0$, $\delta_2' > 0$, $\alpha' = -10°$, $\varphi' = -100°$, and $\text{PDF}'_{LCC} = -0.02$ when the primary and secondary sides are aligned. Fig. 12 shows that PDF_{LCC} changes with $|\delta_1|$ when the additional ΔC_2 is considered. The output power is less than 5% lower than the designed power. The high-order harmonics are not taken into consideration in the given analysis. This will result in an additional error.

The waveforms of the primary and secondary sides at different misalignments are shown in Fig. 13. The maximum efficiency of the designed WPT system is 96% from dc power source to load. When the primary and secondary coils are aligned, the maximum efficiency is 96% at 7.7-kW maximum output power. At a 350-mm misaligned position, the maximum power is 3.7 kW, which is the rated power and will not be achieved by the SS compensation topology using the same coil structure. Fig. 14 shows the efficiencies of different rated power values with different misalignment tolerance levels. The efficiency drops with the decrease in the rated output power, whereas the efficiency of the misaligned system is higher than that of the aligned system at the same lower rated power. The output power is regulated by controlling the input voltage in this work. For low rated power, the input voltage of the system at the aligned position is lower than that of the system at the misaligned position to keep the same rated power. However, the system is designed to have the highest efficiency at the maximum input voltage at the aligned position. Hence, the efficiency will be lower if the system transfers lower power at the aligned position.

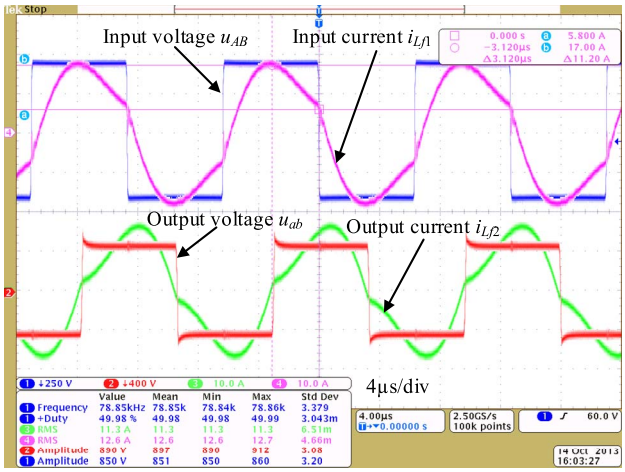

(a)

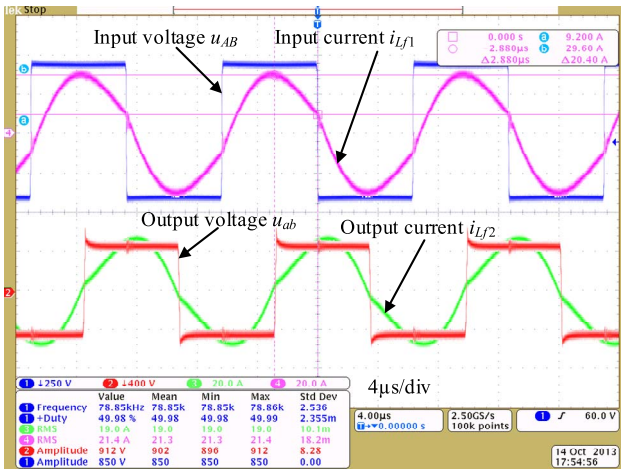

(b)

Fig. 13. Waveforms of input voltage u_{AB} and current i_{Lf1} and output voltage u_{ab} and current i_{Lf2}. (a) Misalignment is 310 mm. (b) Misalignment is 0 mm.

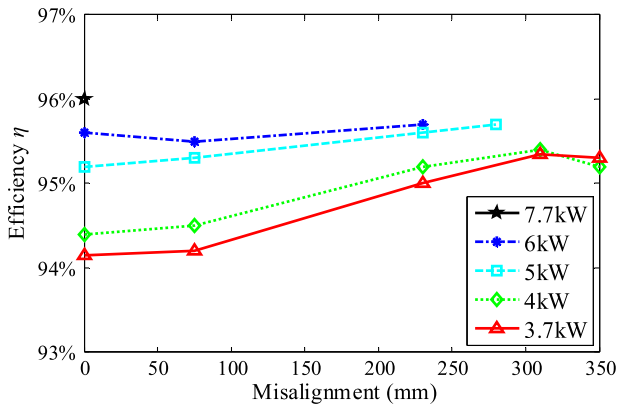

Fig. 14. Experimental efficiency of different rated power values with different misalignments.

VI. Conclusion

In this paper, the double-sided LCC and SS compensation topologies for EV wireless chargers have been analyzed and compared in terms of well-tuned and mistuned conditions. The electrical characteristics of these two topologies are affected by the variations of self-inductances and mutual inductance (ΔL_i and M), and they are coupled together ($\delta_i = \Delta L_i/M$) when the primary and secondary coils are misaligned. The output PDF was proposed to determine the impacts of the load variations when mistuning exists. The theoretical analysis proved that the double-sided LCC compensation topology is less sensitive to the variations of self-inductances caused by the change in the relative position of the primary and secondary coils. The voltage and current stresses on the series capacitors and main coils of the double-sided LCC compensation topology are smaller than those of the SS compensation topology. The efficiency of the double-sided LCC compensation topology is higher and steady, although it is lower than that of the SS compensation topology at higher mutual inductance values. Due to time and funding constraints, we were only able to build one 7.7-kW EV wireless charger prototype that is based on the double-sided LCC topology for experimental validation. The experiment has shown consistent results with the analysis.

References

[1] M. Yilmaz and P. T. Krein, "Review of battery charger topologies, charging power levels, and infrastructure for plug-in electric and hybrid vehicles," *IEEE Trans. Power Electron.*, vol. 28, no. 5, pp. 2151–2169, May 2013.

[2] P. Ning, J. M. Miller, O. C. Onar, C. P. White, and L. D. Marlino, "A compact wireless charging system development," in *Proc. IEEE 28th Annu. APEC Expo.*, 2013, pp. 3045–3050.

[3] S. Choi, J. Huh, W. Lee, and C. Rim, "Asymmetric coil sets for wireless stationary EV chargers with large lateral tolerance by dominant field analysis," *IEEE Trans. Power Electron.*, vol. 29, no. 12, pp. 6406–6420, Dec. 2014.

[4] H. H. Wu, A. Gilchrist, K. Sealy, and D. Bronson, "A 90 percent efficient 5kW inductive charger for EVs," in *Proc. IEEE ECCE*, 2012, pp. 275–282.

[5] G. A. Covic and J. T. Boys, "Inductive power transfer," *Proc. IEEE*, vol. 101, no. 9, pp. 1276–1289, Jun. 2013.

[6] A. Khaligh and S. Dusmez, "Comprehensive topological analysis of conductive and inductive charging solutions for plug-in electric vehicles," *IEEE Trans. Veh. Technol.*, vol. 61, no. 8, pp. 3475–3489, Oct. 2012.

[7] J. Huh, S. W. Lee, W. Y. Lee, G. H. Cho, and C. T. Rim, "Narrow-width inductive power transfer system for online electrical vehicles," *IEEE Trans. Power Electron.*, vol. 26, no. 12, pp. 3666–3679, Dec. 2011.

[8] M. Budhia, J. T. Boys, G. A. Covic, and C.-Y. Huang, "Development of a single-sided flux magnetic coupler for electric vehicle IPT charging systems," *IEEE Trans. Ind. Electron.*, vol. 60, no. 1, pp. 318–328, Jan. 2013.

[9] S. Li and C. Mi, "Wireless power transfer for electric vehicle applications," *IEEE. J. Emerging Sel. Topics Power Electron.*, vol. 3, no. 1, pp. 4–17, Mar. 2015.

[10] S. Cheon *et al.*, "Circuit-model-based analysis of a wireless energy-transfer system via coupled magnetic resonances," *IEEE Trans. Ind. Electron.*, vol. 58, no. 7, pp. 2906–2914, Jul. 2011.

[11] C.-S. Wang, G. A. Covic, and O. H. Stielau, "Power transfer capability and bifurcation phenomena of loosely coupled inductive power transfer systems," *IEEE Trans. Ind. Electron.*, vol. 51, no. 1, pp. 148–157, Feb. 2004.

[12] C.-S. Wang, O. H. Stielau, and G. A. Covic, "Design considerations for a contactless electric vehicle battery charger," *IEEE Trans. Ind. Electron.*, vol. 52, no. 5, pp. 1308–1314, Oct. 2005.

[13] T.-D. Nguyen, S. Li, W. Li, and C. C. Mi, "Feasibility study on bipolar pads for efficient wireless power chargers," in *Proc. IEEE 29th Annu. APEC Expo.*, 2014, pp. 1676–1682.

[14] M. Budhia, G. A. Covic, and J. T. Boys, "Design and optimization of circular magnetic structures for lumped inductive power transfer systems," *IEEE Trans. Power Electron.*, vol. 26, no. 11, pp. 3096–3108, Nov. 2011.

[15] W. Zhang, S.-C. Wong, C. K. Tse, and Q. Chen, "Design for efficiency optimization and voltage controllability of series–series compensated inductive power transfer systems," *IEEE Trans. Power Electron.*, vol. 29, no. 1, pp. 191–200, Jan. 2014.

[16] S. Hasanzadeh and S. Vaez-Zadeh, "Efficiency analysis of contactless electrical power transmission systems," *Energy Convers. Manage.*, vol. 65, pp. 487–496, Jan. 2013.
[17] J. Sallan, J. L. Villa, A. Llombart, and J. F. Sanz, "Optimal design of ICPT systems applied to electric vehicle battery charge," *IEEE Trans. Ind. Electron.*, vol. 56, no. 6, pp. 2140–2149, Jun. 2009.
[18] H. H. Wu, A. Gilchrist, K. D. Sealy, and D. Bronson, "A high efficiency 5 kW inductive charger for EVs using dual side control," *IEEE Trans. Ind. Informat.*, vol. 8, no. 3, pp. 585–595, Aug. 2012.
[19] U. K. Madawala, M. Neath, and D. J. Thrimawithana, "A power–frequency controller for bidirectional inductive power transfer systems," *IEEE Trans. Ind. Electron.*, vol. 60, no. 1, pp. 310–317, Jan. 2013.
[20] F. F. A. Van der Pijl, M. Castilla, and P. Bauer, "Adaptive sliding-mode control for a multiple-user inductive power transfer system without need for communication," *IEEE Trans. Ind. Electron.*, vol. 60, no. 1, pp. 271–279, Jan. 2013.
[21] S. Li, W. Li, J. Deng, T. D. Nguyen, and C. C. Mi, "A double-sided LCC compensation network and its tuning method for wireless power transfer," *IEEE Trans. Veh. Technol.*, vol. 64, no. 6, pp. 2261–2273, Jun. 2015.
[22] J. L. Villa, J. Sallan, J. F. Sanz Osorio, and A. Llombart, "High-misalignment tolerant compensation topology for ICPT systems," *IEEE Trans. Ind. Electron.*, vol. 59, no. 2, pp. 945–951, Feb. 2012.
[23] C.-S. Wang, G. A. Covic, and O. H. Stielau, "Investigating an LCL load resonant inverter for inductive power transfer applications," *IEEE Trans. Power Electron.*, vol. 19, no. 4, pp. 995–1002, Jul. 2004.
[24] U. K. Madawala and D. J. Thrimawithana, "A bidirectional inductive power interface for electric vehicles in V2G systems," *IEEE Trans. Ind. Electron.*, vol. 58, no. 10, pp. 4789–4796, Oct. 2011.
[25] D. J. Thrimawithana and U. K. Madawala, "A generalized steady-state model for bidirectional IPT systems," *IEEE Trans. Power Electron.*, vol. 28, no. 10, pp. 4681–4689, Oct. 2013.
[26] C.-S. Wang, O. H. Stielau, and G. A. Covic, "Load models and their application in the design of loosely coupled inductive power transfer systems," in *Proc. Int. PowerCon Syst. Technol.*, 2000, vol. 2, pp. 1053–1058.
[27] C. Huang, J. James, and G. Covic, "Design considerations for variable coupling lumped coil systems," *IEEE Trans. Power Electron.*, vol. 30, no. 2, pp. 680–689, Feb. 2015.
[28] R. W. Erickson and D. Maksimovic, *Fundamentals of Power Electronics*, 2nd ed. New York, NY, USA: Academic, 2001.
[29] R. Yu, G. K. Y. Ho, B. M. H. Pong, B. W. K. Ling, and J. Lam, "Computer-aided design and optimization of high-efficiency LLC series resonant converter," *IEEE Trans. Power Electron.*, vol. 27, no. 7, pp. 3243–3256, Jul. 2012.

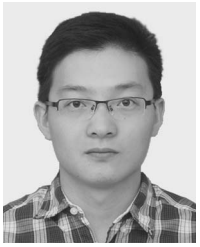

Weihan Li (S'13) received the B.S. degree in automotive engineering from Hefei University of Technology, Hefei, China, in 2010, where he is currently working toward the Ph.D. degree in automotive engineering.

From September 2012 to August 2014, he was a joint Ph.D. student funded by the China Scholarship Council with the GATE Center for Electric Drive Transportation, Department of Electrical and Computer Engineering, University of Michigan, Dearborn, MI, USA, where he is involved in the modeling and design of wireless chargers for electric vehicles (EVs)/plug-in hybrid electric vehicles (PHEVs). His research interests include wireless power transfer, EV/PHEV systems, renewable energy, and power electronics.

Han Zhao received the B.S. and M.S. degrees from Hefei University of Technology, Hefei, China, in 1982 and 1984, respectively, and the Ph.D. degree from Aalborg University, Aalborg, Denmark, in 1990, all in mechanical engineering.

He is the Vice President of Hefei University of Technology. His research interests include mechanical transmission, digital design and manufacturing technology, information systems, dynamics and control, automotive, and electric vehicles.

Junjun Deng (S'13–M'14) received the B.S. and M.S. degrees in electrical engineering from Northwestern Polytechnical University, Xi'an, China, in 2008 and 2011, respectively, where he is currently working toward the Ph.D. degree in electrical engineering.

From 2011 to 2013, he was a joint Ph.D. student funded by the China Scholarship Council with the University of Michigan, Dearborn, MI, USA. From 2013 to 2014, he was a Research Assistant with the Department of Electrical and Computer Engineer, University of Michigan. His research interests include wireless power transfer, resonant power conversion, and high-performance battery chargers for electric vehicles.

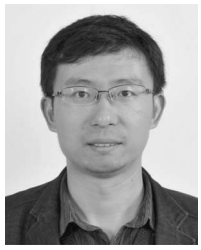

Siqi Li (M'13) received the B.S. and Ph.D. degrees in electrical engineering from Tsinghua University, Beijing, China, in 2004 and 2010, respectively.

From 2011 to 2013, he was a Postdoctoral Fellow with the University of Michigan, Dearborn, MI, USA. In 2013, he joined the Faculty of Electric Power Engineering, Kunming University of Science and Technology, Kunming, China, where he is currently a Lecturer with the Department of Electrical Engineering. He is also the Director of the Advanced Power Electronics and New Energy Laboratory. His research interests include battery management systems and high-performance wired and wireless battery chargers for electric vehicles.

Chunting Chris Mi (S'00–A'01–M'01–SM'03–F'12) received the B.S.E.E. and M.S.E.E. degrees from Northwestern Polytechnical University, Xi'an, China, and the Ph.D. degree from the University of Toronto, Toronto, ON, Canada, all in electrical engineering.

He is a Professor and the Chair of electrical and computer engineering with San Diego State University, San Diego, CA, USA. Previously, he was a Professor with the University of Michigan, Dearborn, MI, USA. Prior to joining the University of Michigan in 2001, he was with General Electric Company, Peterborough, ON. He has conducted extensive research and has published more than 100 journal papers. His research interests include electric drives, power electronics, electric machines, renewable energy systems, and electrical and hybrid vehicles.

Dr. Mi is an Area Editor of the IEEE TRANSACTIONS ON VEHICULAR TECHNOLOGY.